Investigating Intracellular Dynamics of FtsZ Cytoskeleton with Photoactivation Single-Molecule Tracking

Lili Niu and Ji Yu
Center for Cell Analysis and Modeling, Department of Genetics and Developmental Biology, University of Connecticut Health Center, Farmington, Connecticut

ABSTRACT Using photoactivatable fluorescent protein as an intracellular protein label for single-molecule tracking offers several advantages over the traditional methods. Here we demonstrate the technique of photoactivation single-molecule tracking by investigating the mobility dynamics of intracellular FtsZ protein molecules in live *Escherichia coli* cells. FtsZ is a prokaryotic cytoskeleton protein (a homolog of tubulin) and plays important roles in cytokinesis. We demonstrate two heterogeneous subpopulations of FtsZ molecules with distinct diffusional dynamics. The FtsZ molecules forming the Z-rings near the center of the cell were mostly stationary, consistent with the assumption that they are within polymeric filamentous structures. The rest of the FtsZ molecules, on the other hand, undergo Brownian motion spanning the whole cell length. Surprisingly, the diffusion of FtsZ is spatially restricted to helical-shaped regions, implying an energy barrier for free diffusion. Consistently, the measured mean-square displacements of FtsZ showed anomalous diffusion characteristics. These results demonstrated the feasibility and advantages of photoactivation single-molecule tracking, and suggested new levels of complexity in the prokaryotic membrane organization.

INTRODUCTION

Fluorescent proteins (FPs), as fully genetically encoded fluorescent markers, have revolutionized the field of cell biology. In addition, their high fluorescence quantum yields open up the possibility of studying the dynamics of cellular processes by single-molecule tracking (1–5). Compared to popular ensemble techniques, such as fluorescence recovery after photobleaching (FRAP) (6), not only is single-molecule tracking more powerful in resolving the heterogeneity of the molecular population, it also provides higher spatial accuracy (7,8), based on the principle of centroid determination (9). The latter advantage is particularly important for studying molecules in small cells, such as bacteria; or molecules confined in a small compartment, such as the mitochondria. On the other hand, even though sensitive microscopes capable of single-molecule detection can now be easily constructed with off-the-shelf components, we have not seen them being widely used in cell biology studies, due to at least two technical problems. Firstly, fluorescent proteins often have a fast photobleaching rate (10), making it difficult to track molecules for an extended period of time. Secondly, single molecule detection in a cell requires stringent control of the expression level to be very low, so that the molecules of interest are spatially separated from each other and being detected individually. Such a requirement, however, is often incompatible with the expression systems used in cell biology today, which usually are optimized for high-level expression. To overcome these two problems, we devised a technique that we call photoactivation single-molecule tracking. In this system, a photoactivatable fluorescent protein (PAFP), Dendra2 (11), is used as the single-molecule label, and the number of fluorescent protein molecules controlled by photoactivation instead of protein expression.

Dendra2 is a monomeric photoactivatable fluorescent protein, which is capable of an irreversible photoconversion from the native green fluorescent state (emission maximum at 507 nm) to a photoactivated red fluorescent state (emission maximum at 573 nm), upon illumination with UV-violet light (e.g., 405 nm). We have set up a single-molecule tracking microscope, in which only the photoactivated molecules are detected. Under a low-level exposure to photoactivation laser illumination of 405 nm, a few fluorescent protein molecules within the sample would be activated, which could in turn be detected individually. The number of fluorescent protein molecules that are detected in the cell at any time, therefore, is not simply controlled by the protein expression level, but also by the photoactivation dosage (activation laser power times the duration). The latter is much more predictable and easier to adjust. Thus, simple plasmid expression systems could be used and no tedious optimization of the expression level is necessary. To obtain longer time traces of single molecules, our strategy is simply to increase the data collection throughput. Photobleaching is a stochastic process—each individual molecule will last for a different amount of time before photobleaching. With a large data set, results from a fraction of the molecules are expected to last much longer and therefore be useful for analyzing the long-time correlation of the underlying molecular process. With photoactivatable fluorescent proteins, new fluorescent molecules can be regenerated continuously for imaging at the same sample. Thus, a simple automated microscope can be set up to repeat the photoactivation/imaging cycles thousands of

Submitted February 7, 2008, and accepted for publication March 27, 2008.

Address reprint requests to Ji Yu, Tel.: 860-679-7680; E-mail: jyu@uchc.edu.

Editor: Petra Schwille.

0006-3495/08/08/2009/08 $2.00

doi: 10.1529/biophysj.108.128751

times, without much need of human intervention. Such an approach offers significantly higher data collection throughput compared to earlier experiments utilizing single-color fluorescent proteins.

To demonstrate the mechanism of this system, we present here a case study of FtsZ, a prokaryotic homolog of tubulin (12,13), using photoactivation single-molecule tracking in live *Escherichia coli* cells. FtsZ is a major component of the prokaryotic cytoskeleton and plays important roles in cytokinesis (14), a process in which the mother cell is divided into two daughter cells. FtsZ is conserved in most bacteria as well as Archaea, chloroplasts, and some mitochondria. Similar to tubulin, FtsZ is a GTPase and is capable of forming long protofilaments by polymerization in a head-to-tail fashion (15). Such a polymerization process has been extensively studied under in vitro conditions (13,16–19). In the exponentially growing cells, a substantial portion of the intracellular FtsZ molecules are localized, presumably in the polymeric filamentous form, underneath the inner membrane at the future division site, forming a compact ringlike structure (20) commonly known as the Z-ring. The Z-ring is considered as a structural scaffold for assembling the complete cytokinesis apparatus, which includes more than a dozen other proteins (21,22). Recent results from more refined optical microscopy studies on various bacterial species have further shown the existence of a helically localized portion of FtsZ molecules (23–26) spanning from one pole of the cell to the other, regardless of the presence of the Z-ring. Very little is known about these FtsZ molecules outside the Z-ring structure. FRAP experiments have demonstrated that the Z-ring is a highly dynamic structure (27,28), but it is not clear how does that corresponds to the dynamics of individual FtsZ molecules.

METHODS

Bacterial culture and plasmid construction

The plasmid encoding chimeric *ftsZ-dendra2* gene is constructed by a standard PCR cloning procedure. The *ftsZ* gene coding sequence is directly amplified from *E. coli* chromosome DNA and *dendra2* DNA is purchased from Axxora (San Diego, CA). The chimeric sequence is then subcloned onto a vector derived from pBAD-ThioE (Invitrogen, Carlsbad, CA) so that the expression of the fusion protein is controlled by the arabinose promoter. The FtsZ domain and Dendra2 linked with a 15 amino-acid sequence (LGGRADPAFLYKVVIKL), which is flexible enough so that we observed no fluorescence polarization anisotropy even from the molecules within the Z-ring (data not shown).

Escherichia coli cells (K12 strain BW25142, obtained from Col: Genetic Stock Center of Yale University, New Haven, CT) transformed with the plasmid were grown in LB media (Sigma-Aldrich, St. Louis, MO) supplemented with appropriate antibiotics (ampicillin: 50 μg/ml) overnight at 37°C. The overnight culture was reinoculated (1:200) into fresh M9 minimal media supplemented with glucose and antibiotics and grown until OD_{600} reaches 0.2, at which point the protein expression is mildly induced by adding arabinose to 0.05% concentration. Cells are imaged after 1 h induction. Under such a condition, the cells keep dividing without noticeable changes in morphology and cell-length, while higher induction levels arrest cell division and causes cells to grow into filamentous shapes. Higher induction also leads to higher fluorescence background even without any photoactivation and therefore was avoided. As a precaution, all cells were grown in dark before imaging.

Single-molecule microscopy

Fluorescence images of *E. coli* cells were taken with a modified epi-fluorescence microscope (model No. IX81, Olympus, Melville, NY). Photoactivation was carried out with a 405-nm diode laser (Cube laser system, Coherent, Santa Clara, CA). The power and duration of the activation laser is analog-controlled by the computer through a D/A conversion interface (model No. NI-USB-6251, National Instruments, Austin, TX). A second 532-nm DPSS diode laser (Lambda Photometrics, Harpenden, UK) is used for fluorescence excitation at a power density of ~0.7 kW/cm^2. A homebuilt

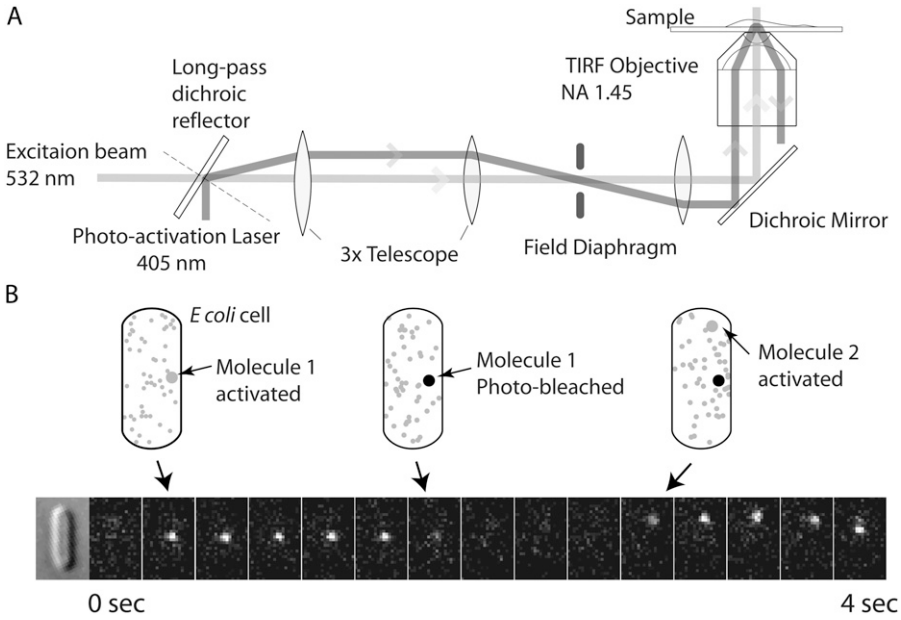

FIGURE 1 Principle of the photoactivation single-molecule tracking method. (*A*) The microscope setup. The photoactivation laser excites the sample under TIR condition. The fluorescence excitation laser illuminates the whole depth of the sample. (*B*) A segment of the fluorescence trajectory taken from *E. coli* cells expressing FtsZ-Dendra2 chimeric protein. The unactivated molecules are illustrated in gray, the activated in red, and the photobleached in black. The first image in the time-series is the differential interference contrast (DIC) image. The rest are fluorescence images shown every 400 ms. The scale bar represents 1 μm.

illumination arm (Fig. 1 *A*) was used to combine the two laser beams into the microscope. The photoactivation light (405 nm) is brought into the system under a through-objective total-internal-reflection (TIR) illumination geometry, so that the membrane-associated FtsZ molecules are preferably excited with the UV light, whereas the fluorescence excitation (532 nm) of the activated fluorescent protein is through a normal wide-field epi-illumination geometry, so that molecules can be followed even after they diffused away from the bottom to the top of the cell. Because the diameter of *E. coli* cells is relative small (800–1000 nm), the whole cell is in focus within the imaging depth of field (~1 μm) of the microscope, without the need to adjust focus.

Cells were immobilized on 1% agarose gel in M9 medium. Images were taken 30 min after mounting the sample on the microscope to allow cells to adapt to the new environment. All images were taken at room temperature. Cells were illuminated with both the 405-nm photoactivation laser and the 532-nm fluorescence excitation laser, so that the photoactivation process and the photobleaching of the activated molecules are balanced to reach a steady state, under which condition the average steady-state number of activated fluorescent molecules is

$$n_{\mathrm{fp}} = \frac{\Phi_{405}\sigma_{405}n_{\mathrm{T}}\phi}{k_{\mathrm{pb}}},$$

where Φ_{405} is the power density of the 405-nm laser in photon flux, σ_{405} is the absorption cross section at 405 nm, n_{T} is the total number of unactivated fluorescent proteins in the illumination field, ϕ is the photoactivation quantum yield, and k_{pb} is the rate constant of photobleaching. The power density of the 405-nm laser was adjusted at the beginning of the experiment to ensure that n_{fp} was a small number (<1 per cell). The laser power was then maintained constant through the experiment. Fluorescence images were taken every 200 ms via a 60× microscope objective (NA = 1.45, Olympus) with 100-ms acquisition time for each image. The fluorescence signal was collected with a TE-cooled EM-CCD camera (PhotonMax, Roper Scientific, Trenton, NJ). The principle of the experimental design is illustrated in Fig. 1 *B*. Image acquisition software is built on top of the μManager platform (http://micro-manager.org). After image collection, the image files are batch-processed by the DiaTrack (Semasopht, Chavannes, Switzerland) software to extract the centroid positions of the detected molecules and construct diffusion trajectories automatically.

Random-walk simulation of the diffusion of FtsZ protein molecules on *E. coli* cell membrane

The diffusion dynamics of FtsZ protein molecules were simulated with random-walking particles in cylindrical coordinates (x, θ), where x denotes the distance along the cell's long axis, and θ denotes the azimuthal angle. The cell shape is assumed be a cylinder with two hemispheres capped on both sides. To compare to experimental measurements, the simulation results were converted into Cartesian coordinates corresponding to the lab frame according to

$$\begin{cases} x_{\mathrm{L}} = x \\ y_{\mathrm{L}} = r\cos\theta \end{cases},$$

where x_{L} and y_{L} are the lab-frame coordinates, and r is the diameter of the cell. For simplicity, the cell is assumed to be cylindrical in shape, with a diameter $r = 0.5$ μm and cell length $L = 2$ μm. Mean-square displacements (MSD) in the lab frame are calculated according to

$$MSD = \langle \Delta x_{\mathrm{L}}^2 + \Delta y_{\mathrm{L}}^2 \rangle,$$

where the brackets denote ensemble averaging. The simulation creates a mapping between *MSD* measured in lab coordinates to the corrected true MSD_{c} according to the two-dimensional free diffusion model,

$$MSD_{\mathrm{c}} = 4Dt = \delta^2 t/t_0 = \delta^2 N,$$

where t_0 is the time spent for each step, N is the number of steps simulated, δ is the step size in simulation, and t is the corresponding time. Typical step size used for simulation varies from 5 to 30 nm. No significant variation of the simulation results was observed under the different step sizes used.

RESULTS AND DISCUSSION

Heterogeneous population of intracellular FtsZ-Dendra2 molecules

The ensemble fluorescence signal from FtsZ-Dendra2 proteins expressed in *E. coli* can be detected with a standard epi-fluorescence microscopy with 488-nm excitation (shown in Fig. 2 *A*). The localization pattern is very similar to previous reports of FtsZ using either green fluorescent protein as a fluorescent marker (23) or using immunofluorescence staining (29). A bright Z-ring structure can be seen at the midcell position and a weaker periodical structure is observed for the peripheral FtsZ molecules outside the midcell region. The peripheral FtsZ molecules are thought to form a filamentous helical structure underneath the membrane, as illustrated in Fig. 2 *B*. Although cytoplasmic FtsZ molecules might also exist, it has been shown that single-molecule imaging of cytoplasmic proteins requires stroboscopic excitations (3,30) due to their fast diffusion rate (27). Under our imaging condition (100 ms exposure time), freely diffusing molecules in the cytoplasm would be blurred out in the image. Consequently, activation of the cytoplasmic FtsZ molecules will increase the overall fluorescence background of the cell. Therefore, a TIR photoactivation is applied to minimize the possibility of photoactivating cytoplasmic molecules.

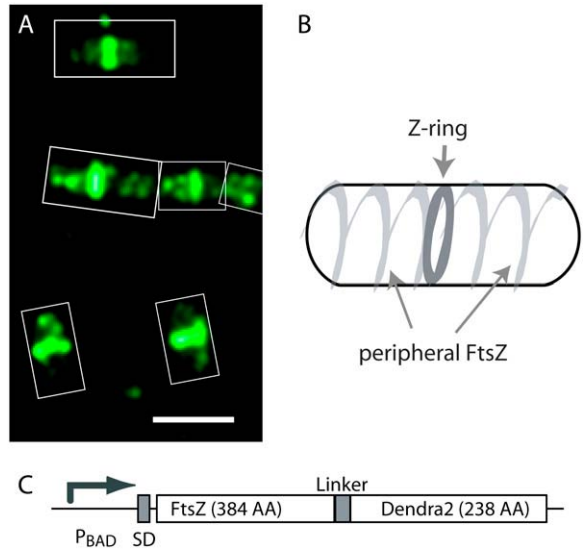

FIGURE 2 Localization of FtsZ-Dendra2 proteins in *E. coli* cells. (*A*) Green fluorescence from the unactivated proteins in *E. coli* cells. Each cell is highlighted by the rectangular boxes. The scale bar represents 2 μm. (*B*) A schematic representation of the FtsZ localization pattern observed in literature using fluorescence microscopy. The central dark ring represents the Z-ring. The helix represents the FtsZ molecules outside the Z-ring. (*C*) Chimeric construct of ftsZ-dendra2 expression. SD, Shine-Dalgarno sequence.

Under exposure to weak 405-nm photoactivation, single FP molecules can be detected and their diffusion trajectories in the cells can be recorded. Typically, >1000 single molecules can be detected in one continuous recoding. The large dataset allows for detailed analysis of the molecular behaviors. Plotted in Fig. 3 is a histogram of single molecules' spatial displacements within a short time interval (200 ms, the time delay in the timelapse imaging). The figure shows two distinct groups of molecules, evident from the dual peaks in the histogram. The overall distribution can be roughly fitted with the sum of two terms,

$$P(r) = a_1 r e^{-r^2/s_1^2} + a_2 r e^{-r^2/s_2^2},$$

where r is the displacements. The function is chosen because the probability density of the displacements in an ideal two-dimensional random-walk model follows the functional form of $p_r \propto r e^{-r^2/s^2}$ (31).

The first peak in the distribution corresponds to a subset of molecules with an average nominal displacement of ~30 nm, which is close to the measurement error in extracting the centroid position of single molecule spots. Therefore, we consider these molecules as stationary. The second peak corresponds to a group of molecules that have an average step-size of 210 nm, which is much bigger than the uncertainty in the centroid position measurements. We therefore designate these as mobile FtsZ molecules.

Fig. 4 shows the photobleaching statistics of the FtsZ-Dendra2 molecules. It is apparent that most molecules photobleached quickly, i.e., within 1-s time of exposure to the fluorescence excitation light. However, longer-time trajectories can be obtained by measuring a large number of molecules (a total of 3150 trajectories were analyzed for the histogram). The photobleaching time distribution does not fit well with a single-exponential model (Fig. 4). Even though majority of the data fall under one exponential decay function ($\tau = 720$ ms), it is evident that a slow decaying tail exists in the distribution. The heterogeneity in photobleaching kinetics, however, has no correlation with their mobility; therefore, both stationary and mobile FtsZ-Dendra2 molecules have a long tail in their photobleaching time distributions (data not shown).

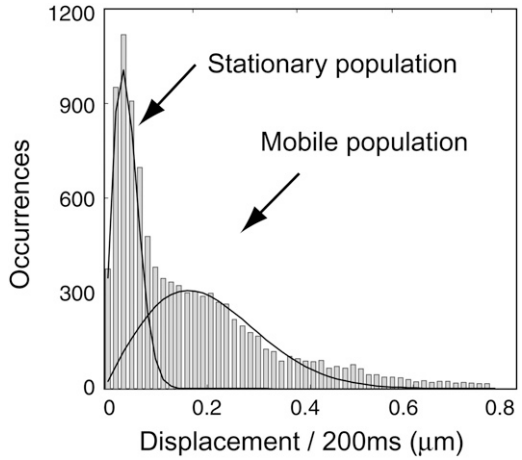

FIGURE 3 The distribution of single FtsZ-Dendra2 molecules' stepping sizes at 200-ms time-interval. The results showed two distinct populations. The solid curves are least-square fitting of the distribution to the function form of $a_1 r e^{-r^2/s_1^2} + a_2 r e^{-r^2/s_2^2}$. The first term represented the stationary population of the molecules. The second represented the mobile population. The two terms of the equation are plotted separately for clarity.

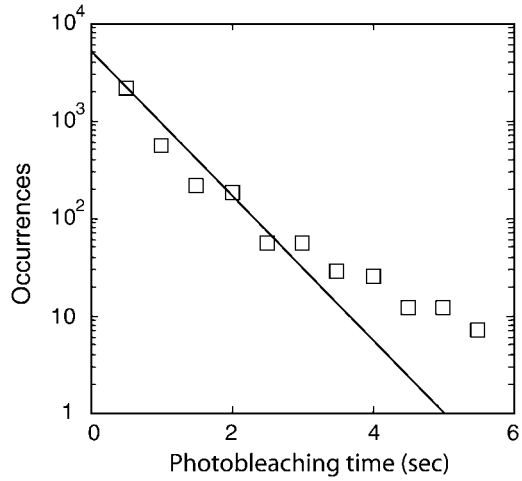

FIGURE 4 Distribution of the single molecule photobleaching times. Histogram of FtsZ-Dendra2 photobleaching time is measured from >3000 molecules under excitation density of 450 W/cm^2. The straight line represented the single exponential fit of the histogram.

Polymeric FtsZ molecules of Z-ring are stationary

Fig. 5 *A* shows two examples of the single molecule time trajectories from the FtsZ molecules that are within the stationary subpopulation (see Fig. 3). (More examples can be seen in Supplementary Material, Movie S1 and Movie S2.) A quick visual inspection suggested that the molecules were seen near the center of the rod-shaped cells. Further analysis of these stationary molecules indeed showed that they were predominately located at the center of the cell (Fig. 5 *B*) and, to a much less degree, at the cell poles—the expected locations of the Z-rings (32). Therefore, we designated these stationary molecules as the FtsZ protein molecules within the Z-ring. The fact that they are immobile is a confirmation of the common assumption that the Z-ring comprises of the polymeric FtsZ filaments (33), which were previously seen in vitro as head-to-tail polymerized linear chains.

Fig. 5 *C* shows the MSD of stationary FtsZ molecules versus time. The apparent displacement observed does not increase with longer time delays; therefore, it is not caused by true molecular movement. Instead, we attribute it to the errors in molecular positions determined with the centroid fitting algorithm. We note that this error (~30 nm) is much smaller than the true diffraction-limited spatial resolution of the op-

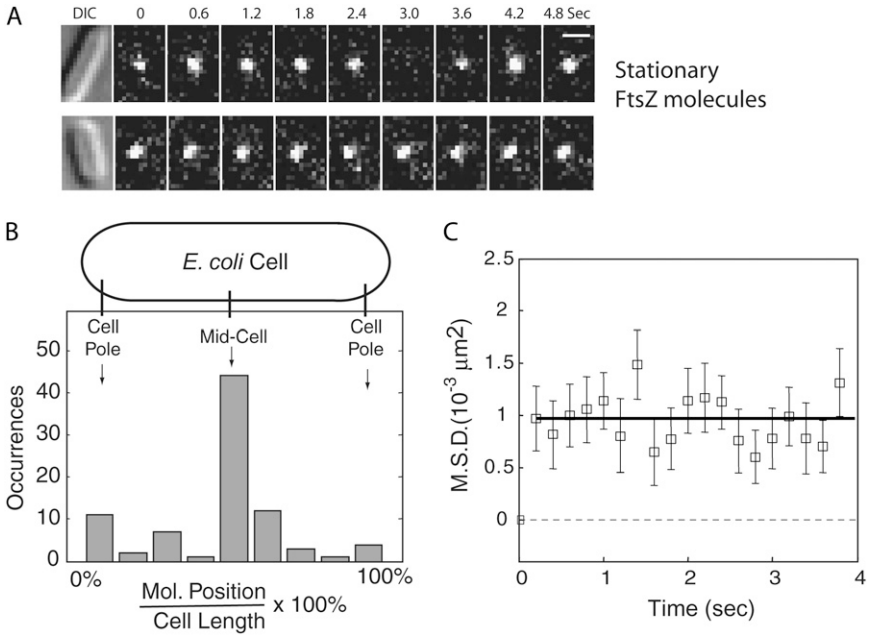

FIGURE 5 Single-molecule trajectories of stationary FtsZ molecules. (*A*) Two examples of fluorescence timelapse images of the stationary FtsZ single molecules shown at 600-ms interval. The first frame shows the DIC images of the cell. (*B*) Spatial distribution of the stationary FtsZ molecules within the cell. Most of the stationary FtsZ molecules are located at the center of the cell. (*C*) Mean-square displacement of stationary FtsZ molecules calculated from ~800 trajectories showing a constant number representing the measurement noise.

tical system (~300 nm), reflecting the general capability of single molecule detection to achieve spatial accuracy beyond the diffraction limit.

It is interesting to consider our result in comparison with previously FRAP studies of the Z-ring in bacteria (27,28), which had showed that Z-rings are highly dynamic structures. The fluorescence of a photobleached Z-ring in *E. coli*, for example, would quickly recover with a time-constant of ~9 s. The result indicates that the filaments in Z-rings are undergoing continuous remodeling. Based on our results from single molecule imaging, we can further conclude that all the remodeling is carried out through a dynamic equilibrium between the polymerization and depolymerization reactions. In other words, there is no net sliding motion in between the filaments themselves.

FtsZ molecules outside Z-ring undergo anomalous diffusion

The second peak in Fig. 3 corresponds to the molecules that are diffusing in a random-walk type of motion spanning the whole cell (Fig. 6 *A*, Movie S3, Movie S4, Movie S5, and Movie S6). Since FtsZ is a tubulin homolog and considered a cytoskeleton molecule, we first examined whether the

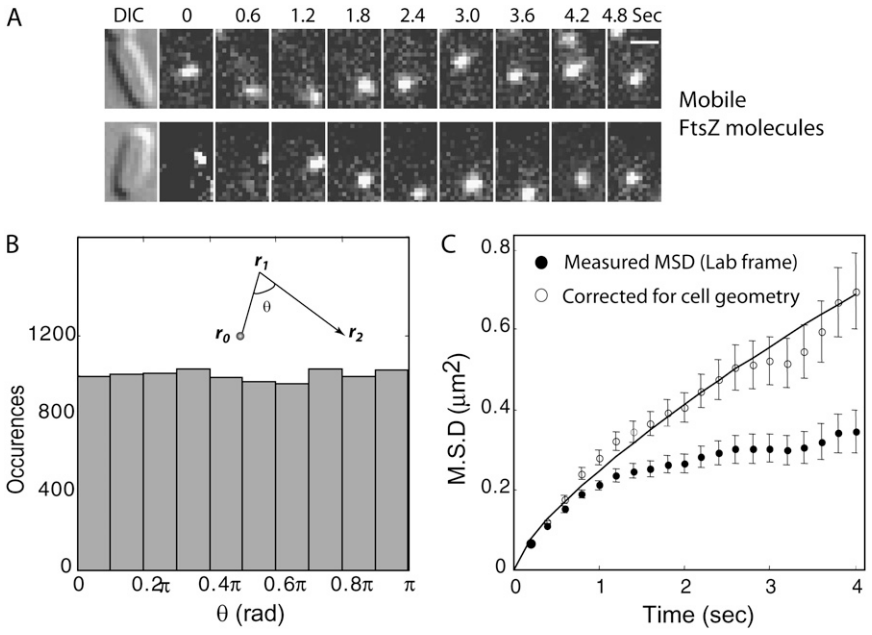

FIGURE 6 Single-molecule trajectories of mobile FtsZ molecules. (*A*) Two examples of timelapse images of the mobile FtsZ single molecules shown at 600 ms interval. The first frame shows the DIC images of the cell. (*B*) The distribution of the angles between two consecutive displacement steps from a mobile FtsZ molecule. The histogram shows a uniform distribution between 0 and π, suggesting that treadmilling is of little effect in driving the movement of FtsZ. (*C*) MSD of mobile FtsZ molecules calculated from >2000 trajectories. The raw measurements in lab coordinates are plotted in solid circles. The corrected MSD based on computer simulation is plotted in open circles. The solid line is the best fit to the anomalous diffusion model.

movements are driven or partially driven by treadmilling: the directional movement of cytoskeleton molecules due to the constant polymerization at one end of the filament and depolymerization at the other. In fact, MreB—the bacterial homolog of actin—was previously shown to have treadmilling dynamics (30), albeit at a much slower speed. To test this hypothesis, we evaluated the correlation between consecutive movement steps of single molecules by calculating the angle between two consecutive displacement steps,

$$\theta = \arccos\left(\frac{\vec{r}_t \cdot \vec{r}_{t-1}}{|\vec{r}_t| \times |\vec{r}_{t-1}|}\right),$$

where $\vec{r}_t$ denotes the displacement vector of a molecule at time step t. Fig. 6 *B* displays the distribution of θ of mobile molecules. For highly correlated motion of treadmilling, we should expect θ to be highly concentrated at near 0 or π. Instead, the measured θ-values distribute uniformly among all possible values between 0 and π. Based on this result, we conclude that the mobile FtsZ molecules are not undergoing treadmilling, as would be expected from a highly polymeric form.

Longer timescale dynamics of FtsZ are further evaluated with MSD of the mobile molecules (Fig. 6 *C*). The two-dimensional MSD is most readily interpreted for diffusion on a flat surface. The FtsZ proteins imaged, however, are associated with the cell membrane, which is a capsule-shaped surface instead of a flat two-dimensional plane. It has been pointed out by Deich et al. (1) that such a MSD measurement at laboratory frame is distorted by the cell shape. The experimental measurements therefore are compared to computer simulations to correct for the effect of the cell surface (1). The resulting normalized MSD (Fig. 6 *C*) should scale linearly with time if the dynamics is free diffusion on a flat energy surface. Our measurement, on the other hand, shows a sublinear relationship between MSD and time. The data can be fit with an anomalous diffusion model (34,35), using a time-dependent diffusion coefficient,

$$D = (1/4)\Gamma t^{1-\alpha}$$
$$MSD = 4DT = \Gamma t^{\alpha},$$

where *MSD* scales versus time to the power of α, which is smaller than one. We obtained that $\alpha = 0.74 \pm 0.05$, and $\Gamma = 0.25 \pm 0.03\ \mu m^2/s^{0.74}$. These results suggested diffusion barriers on the cell membrane hindered the free movement of the molecules. Although we also note that physical meanings of α and Γ cannot be directly inferred from theories based on two-dimensional diffusion, because the *MSD* here is not directly measured but obtained from computer simulation, it is interesting to compare the mobility of FtsZ with some other membrane proteins in bacterial cells. At the distance scale of the cell, e.g., 1 μm, the mobility of the FtsZ molecules is equivalent to a free-diffusing molecule with a diffusion coefficient $D = 0.10\ \mu m^2/s$, which is very similar to the diffusion constant of many monomeric bacterial membrane proteins (1,30,36).

Spatial distribution of mobile FtsZ-Dendra2 molecules is nonuniform in cells

The diffusive characteristic of FtsZ molecules was a surprise. In many species of bacteria, FtsZ molecules outside the Z-rings form a spiral localization pattern (23–26), which had been viewed as the evidences for the hypothesis that FtsZ molecules outside Z-ring form polymeric filaments, similar in structure to the polymeric filaments in Z-rings. Our result, however, showed that these molecules have distinct dynamics from the Z-ring molecules and are most likely in the monomeric or the oligomeric forms, which allow for random diffusions. To further test this, we sorted out all single molecule images that contains mobile FtsZ molecules, and overlaid all these images into one (Fig. 7 *A*). Interestingly, while the fluorescence signals are from many independent single molecules, the overlay images show helical-like patterns across the cell (see Fig. 7, *B* and *C*). To further eliminate

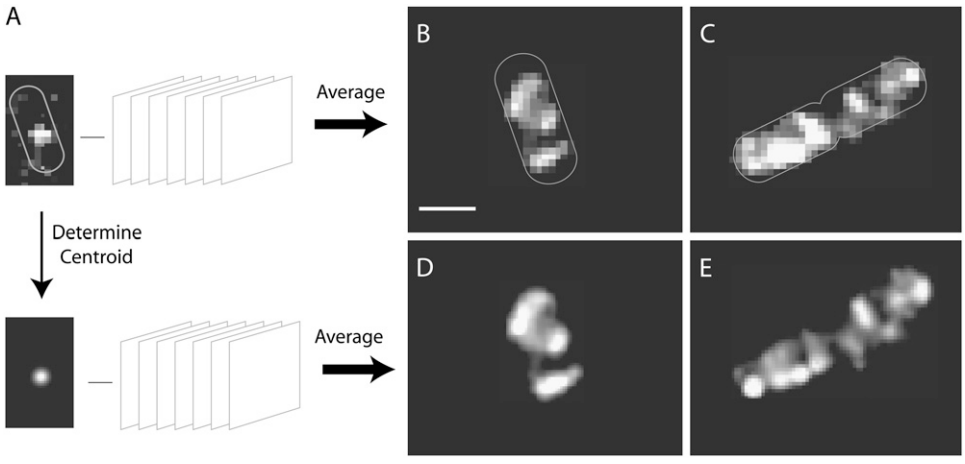

FIGURE 7 Helical spatial pattern of the mobile FtsZ molecules. (*A*) Schemes illustrating the process for obtained overlay images from single molecule data. (*B* and *C*) Images of cells obtained by overlaying many single-molecule images of the mobile FtsZ molecules from the same cell. The images showed spiral-shaped patterns indicating the diffusion of FtsZ is limited to these regions. (*D* and *E*) Images of cells obtained by overlaying Gaussian spots of 300 nm, which are placed at the same centroid positions of detected single mobile FtsZ molecules. Each image is constructed from >300 single-molecule images collected within a timespan of 3 min.

the possibility that such a helical pattern is due to a residual background signal that is present in all single molecule images, the overlay images are compared to constructed images based on single molecule centroid determination. Specifically, the centroid positions of mobile molecules are extracted from each image. We then replaced the original images with constructed images, in which a two-dimensional Gaussian peak is plotted at the same centroid positions to represent an ideal image of a single molecule. The width of the Gaussian peak is 300 nm, corresponding to the width of point-spread-function of the optical microscope, and the height of the peak is fixed. The practice is similar to the recently published FPALM methods for high-resolution imaging in living cells (37), except a much smaller Gaussian spot is use in Hess et al. (37) to represent each molecule. In our experiment, however, we cannot justify the use of smaller spots due to the much higher mobility of the protein molecules under study. When we overlay all the constructed images, the spiral pattern is again apparent (Fig. 7, *D* and *E*). The small difference in the appearances is mainly due to the fact that molecules have different intensities in the original images while they have an equal intensity in the constructed images. This result confirms that the mobile single molecules we detected are indeed FtsZ molecules that were seen in the spiral patterns. This observation is consistent with the dynamics measurements, which showed that their movements are not free.

Because the FtsZ molecules we observed are constantly moving, the spiral localization pattern has to be dynamically formed. One possible model is that the polymerization and the depolymerization of FtsZ molecules to and from the helical filament is very fast. Since our measurements were limited to slower timescale (hundreds of milliseconds), only the diffusive part of the dynamics is observed. The polymerization and depolymerization reactions perturbed the free diffusion of the FtsZ molecule. An alternative interpretation is that such spiral localization pattern is due to a preexisting membrane structure that is helical, which serves as a diffusion barrier for FtsZ. In other words, the spiral localization of FtsZ reflects the complexity of cell membrane, as opposed to the polymeric filaments of FtsZ themselves. We note that recent imaging experiments have unveiled many membrane-associated protein assemblies that seem to be helical in nature, including some proteins that clearly have no polymerization capability (38). We suspect that there might be a diverse set of different mechanisms for these structures, which clearly deserves further exploration.

CONCLUSION

Bacteria possess substantial intracellular structures organized around various cytoskeleton elements that are highly dynamic in nature. Our analysis of FtsZ mobility suggested that the dynamics of FtsZ molecules is heterogeneous. The mobile part of the molecular population undergoes restricted diffusion—a type of dynamics that has often been seen among eukaryotic membrane proteins (39,40), but has not be widely observed in bacteria species. These results demonstrated the usefulness of the photoactivation single-molecule tracking technique.

During the reviewing process of this article, a brief communication was published by Manley et al. (41) describing a technique similar to the one applied in this study. Despite their short history, PAFPs have already been the basis of several new imaging techniques (8,42,43), which were largely the inspirations for this work. We believe more image modalities using PAFPs will emerge and will provide new insights into the working of biological cells.

We thank Dr. Johan Elf, Dr. Gregory Huber, and Jinying Li for critical readings of the manuscript.

This research is funded by a startup grant from the University of Connecticut Health Center to J.Y.

REFERENCES

1. Deich, J., E. M. Judd, H. H. McAdams, and W. E. Moerner. 2004. Visualization of the movement of single histidine kinase molecules in live *Caulobacter* cells. *Proc. Natl. Acad. Sci. USA*. 101:15921–15926.
2. Douglass, A. D., and R. D. Vale. 2005. Single-molecule microscopy reveals plasma membrane microdomains created by protein-protein networks that exclude or trap signaling molecules in T cells. *Cell*. 121:937–950.
3. Elf, J., G. W. Li, and X. S. Xie. 2007. Probing transcription factor dynamics at the single-molecule level in a living cell. *Science*. 316: 1191–1194.
4. Harms, G. S., L. Cognet, P. H. Lommerse, G. A. Blab, and T. Schmidt. 2001. Autofluorescent proteins in single-molecule research: applications to live cell imaging microscopy. *Biophys. J.* 80:2396–2408.
5. Ober, R. J., C. Martinez, X. Lai, J. Zhou, and E. S. Ward. 2004. Exocytosis of IgG as mediated by the receptor, FcRn: an analysis at the single-molecule level. *Proc. Natl. Acad. Sci. USA*. 101:11076–11081.
6. White, J., and E. Stelzer. 1999. Photobleaching GFP reveals protein dynamics inside live cells. *Trends Cell Biol.* 9:61–65.
7. Yildiz, A., and P. R. Selvin. 2005. Fluorescence imaging with one nanometer accuracy: application to molecular motors. *Acc. Chem. Res.* 38:574–582.
8. Betzig, E., G. H. Patterson, R. Sougrat, O. W. Lindwasser, S. Olenych, J. S. Bonifacino, M. W. Davidson, J. Lippincott-Schwartz, and H. F. Hess. 2006. Imaging intracellular fluorescent proteins at nanometer resolution. *Science*. 313:1642–1645.
9. Thompson, R. E., D. R. Larson, and W. W. Webb. 2002. Precise nanometer localization analysis for individual fluorescent probes. *Biophys. J.* 82:2775–2783.
10. Yu, J., J. Xiao, X. Ren, K. Lao, and X. S. Xie. 2006. Probing gene expression in live cells, one protein molecule at a time. *Science*. 311:1600–1603.
11. Gurskaya, N. G., V. V. Verkhusha, A. S. Shcheglov, D. B. Staroverov, T. V. Chepurnykh, A. F. Fradkov, S. Lukyanov, and K. A. Lukyanov. 2006. Engineering of a monomeric green-to-red photoactivatable fluorescent protein induced by blue light. *Nat. Biotechnol.* 24:461–465.
12. Margolin, W. 2005. FtsZ and the division of prokaryotic cells and organelles. *Nat. Rev. Mol. Cell Biol.* 6:862–871.
13. Romberg, L., and P. A. Levin. 2003. Assembly dynamics of the bacterial cell division protein FTSZ: poised at the edge of stability. *Annu. Rev. Microbiol.* 57:125–154.
14. Errington, J., R. A. Daniel, and D. J. Scheffers. 2003. Cytokinesis in bacteria. *Microbiol. Mol. Biol. Rev.* 67:52–65.
15. Lowe, J., and L. A. Amos. 1998. Crystal structure of the bacterial cell-division protein FtsZ. *Nature*. 391:203–206.

16. Bramhill, D., and C. M. Thompson. 1994. GTP-dependent polymerization of *Escherichia coli* FtsZ protein to form tubules. *Proc. Natl. Acad. Sci. USA.* 91:5813–5817.

17. Lu, C., M. Reedy, and H. P. Erickson. 2000. Straight and curved conformations of FtsZ are regulated by GTP hydrolysis. *J. Bacteriol.* 182:164–170.

18. Mukherjee, A., and J. Lutkenhaus. 1998. Dynamic assembly of FtsZ regulated by GTP hydrolysis. *EMBO J.* 17:462–469.

19. Mingorance, J., S. Rueda, P. Gomez-Puertas, A. Valencia, and M. Vicente. 2001. Escherichia coli FtsZ polymers contain mostly GTP and have a high nucleotide turnover. *Mol. Microbiol.* 41:83–91.

20. Bi, E. F., and J. Lutkenhaus. 1991. FtsZ ring structure associated with division in Escherichia coli. *Nature.* 354:161–164.

21. Lutkenhaus, J., and S. G. Addinall. 1997. Bacterial cell division and the Z ring. *Annu. Rev. Biochem.* 66:93–116.

22. Weiss, D. S. 2004. Bacterial cell division and the septal ring. *Mol. Microbiol.* 54:588–597.

23. Thanedar, S., and W. Margolin. 2004. FtsZ exhibits rapid movement and oscillation waves in helix-like patterns in *Escherichia coli*. *Curr. Biol.* 14:1167–1173.

24. Thanbichler, M., and L. Shapiro. 2006. MipZ, a spatial regulator coordinating chromosome segregation with cell division in *Caulobacter*. *Cell.* 126:147–162.

25. Ben-Yehuda, S., and R. Losick. 2002. Asymmetric cell division in B. subtilis involves a spiral-like intermediate of the cytokinetic protein FtsZ. *Cell.* 109:257–266.

26. Peters, P. C., M. D. Migocki, C. Thoni, and E. J. Harry. 2007. A new assembly pathway for the cytokinetic Z ring from a dynamic helical structure in vegetatively growing cells of *Bacillus subtilis*. *Mol. Microbiol.* 64:487–499.

27. Stricker, J., P. Maddox, E. D. Salmon, and H. P. Erickson. 2002. Rapid assembly dynamics of the *Escherichia coli* FtsZ-ring demonstrated by fluorescence recovery after photobleaching. *Proc. Natl. Acad. Sci. USA.* 99:3171–3175.

28. Anderson, D. E., F. J. Gueiros-Filho, and H. P. Erickson. 2004. Assembly dynamics of FtsZ rings in *Bacillus subtilis* and *Escherichia coli* and effects of FtsZ-regulating proteins. *J. Bacteriol.* 186:5775–5781.

29. Stricker, J., and H. P. Erickson. 2003. In vivo characterization of *Escherichia coli* ftsZ mutants: effects on Z-ring structure and function. *J. Bacteriol.* 185:4796–4805.

30. Kim, S. Y., Z. Gitai, A. Kinkhabwala, L. Shapiro, and W. E. Moerner. 2006. Single molecules of the bacterial actin MreB undergo directed treadmilling motion in *Caulobacter crescentus*. *Proc. Natl. Acad. Sci. USA.* 103:10929–10934.

31. Cherry, R. J., P. R. Smith, I. E. Morrison, and N. Fernandez. 1998. Mobility of cell surface receptors: a re-evaluation. *FEBS Lett.* 430: 88–91.

32. Levin, P. A., and R. Losick. 1996. Transcription factor Spo0A switches the localization of the cell division protein FtsZ from a medial to a bipolar pattern in *Bacillus subtilis*. *Genes Dev.* 10:478–488.

33. Mukherjee, A., and J. Lutkenhaus. 1994. Guanine nucleotide-dependent assembly of FtsZ into filaments. *J. Bacteriol.* 176:2754–2758.

34. Saxton, M. J., and K. Jacobson. 1997. Single-particle tracking: applications to membrane dynamics. *Annu. Rev. Biophys. Biomol. Struct.* 26:373–399.

35. Saxton, M. J. 2007. A biological interpretation of transient anomalous subdiffusion. I. Qualitative model. *Biophys. J.* 92:1178–1191.

36. Mullineaux, C. W., A. Nenninger, N. Ray, and C. Robinson. 2006. Diffusion of green fluorescent protein in three cell environments in *Escherichia coli*. *J. Bacteriol.* 188:3442–3448.

37. Hess, S. T., T. J. Gould, M. V. Gudheti, S. A. Maas, K. D. Mills, and J. Zimmerberg. 2007. Dynamic clustered distribution of hemagglutinin resolved at 40 nm in living cell membranes discriminates between raft theories. *Proc. Natl. Acad. Sci. USA.* 104:17370–17375.

38. Shiomi, D., M. Yoshimoto, M. Homma, and I. Kawagishi. 2006. Helical distribution of the bacterial chemoreceptor via colocalization with the Sec protein translocation machinery. *Mol. Microbiol.* 60:894–906.

39. Vereb, G., J. Szollosi, J. Matko, P. Nagy, T. Farkas, L. Vigh, L. Matyus, T. A. Waldmann, and S. Damjanovich. 2003. Dynamic, yet structured: the cell membrane three decades after the Singer-Nicolson model. *Proc. Natl. Acad. Sci. USA.* 100:8053–8058.

40. Kusumi, A., C. Nakada, K. Ritchie, K. Murase, K. Suzuki, H. Murakoshi, R. S. Kasai, J. Kondo, and T. Fujiwara. 2005. Paradigm shift of the plasma membrane concept from the two-dimensional continuum fluid to the partitioned fluid: high-speed single-molecule tracking of membrane molecules. *Annu. Rev. Biophys. Biomol. Struct.* 34:351–378.

41. Manley, S., J. M. Gillette, G. H. Patterson, H. Shroff, H. F. Hess, E. Betzig, and J. Lippincott-Schwartz. 2008. High-density mapping of single-molecule trajectories with photoactivated localization microscopy. *Nat. Methods.* 5:133–134.

42. Hofmann, M., C. Eggeling, S. Jakobs, and S. W. Hell. 2005. Breaking the diffraction barrier in fluorescence microscopy at low light intensities by using reversibly photoswitchable proteins. *Proc. Natl. Acad. Sci. USA.* 102:17565–17569.

43. Flors, C., J. Hotta, H. Uji-i, P. Dedecker, R. Ando, H. Mizuno, A. Miyawaki, and J. Hofkens. 2007. A stroboscopic approach for fast photoactivation-localization microscopy with *Dronpa* mutants. *J. Am. Chem. Soc.* 129:13970–13977.